Proceedings of the Seventh International Conference on
Railway Technology: Research, Development and Maintenance
Edited by: J. Pombo
Civil-Comp Conferences, Volume 15, Paper 18.7
Civil-Comp Press, Edinburgh, United Kingdom, 2026
ISSN: 2753-3239, doi: 10.4203/ccc.15.18.7


# Effect of Unsupported Sleepers on Wheel Impact Load Detector Performance

**N. Lagata[1], J. C. O. Nielsen[1], M. Maglio[2] and T. Vernersson[1]**

**[1] Department of Mechanical Engineering/CHARMEC, Chalmers University of Technology, Gothenburg, Sweden**
**[2] Trafikverket, Gothenburg, Sweden**

## Abstract

Wheel–rail impact loads caused by discrete wheel tread irregularities, such as wheel flats, can lead to severe damage to both vehicles and track infrastructure. To monitor wheel out-of-roundness, peak loads are commonly measured using wheel impact load detectors. Depending on the detector type, these peak loads may, for example, be derived from post-processing of recorded rail shear forces, rail seat loads, or rail rotations. To ensure accurate load measurements, minimise operational costs, and avoid unnecessary stopping of trains, the detectors must be robust and reliable. This numerical study investigates how unsupported (voided) sleepers within the detector area influence the resulting wheel–rail contact force signature and the unprocessed (raw) sensor signals in the presence of a wheel flat. The analysis considers void depths of up to 4 mm beneath two adjacent sleepers. The effect of unsupported sleepers is analysed through numerical simulations using the in-house software DIFF, in which the dynamic vehicle–track interaction is solved in the time domain. The results show that rail rotation and rail seat load are the most affected by unsupported sleepers, as the increased local track flexibility alters the sleeper–ballast interaction and influences the load distribution along the detector.

**Keywords:** dynamic vehicle–track interaction, wheel flat, wheel impact load detector, unsupported sleeper, rail seat load, rail rotation.

# 1 Introduction

The dynamic interaction between railway vehicles and the track, when wheels include out-of-roundness damage, such as wheel flats or rolling contact fatigue clusters, is characterised by high impact loads. The most severe impacts arise from momentary loss of wheel–rail contact at the tread defect location. Subsequently, as the wheel continues to rotate, it drops onto the rail, while the rail deflects upwards until contact is re-established, thereby generating substantial impact forces [1]. The produced impacts accelerate track deterioration and reduce wheelset durability due to the elevated forces and stresses they induce compared with those associated with undamaged wheels [2].

To mitigate traffic disruptions while maintaining safety, accurate and robust wheel impact load detectors (WILDs) installed along the track should be employed and the consequences of wheel out-of-roundness on the vehicle–track interaction analysed. According to current regulations by the Swedish Transport Administration, Trafikverket, an alarm limit of 350 kN is specified for both passenger coaches and freight wagons. If the maximum load measured by a WILD exceeds this value, the train must travel at a reduced speed to the nearest passing siding, where it is stopped to perform a visual inspection of the wheel. If a wheel tread damage exceeding 60 mm in length is observed, the vehicle must be uncoupled and the wheel maintained [3]. Such operational interventions inevitably lead to traffic disruption, delays, and additional costs.

A previous study has shown that the loads measured by different WILDs, for a given wheel flat, exhibit large scatter and variability, as they are influenced by the condition of the track in the detector area, including both geometry and stiffness [4]. Moreover, as demonstrated in [5] and [6], additional parameters such as train speed, running direction, axle load, and lateral wheel–rail contact position also influence the signals recorded by WILDs. Another finding in [5] is that defect length alone is not a reliable indicator of impact severity: even wheel flats exceeding the prescribed 60 mm limit were found not to generate load levels approaching the 350 kN alarm threshold. Instead, the dominant factors are the defect depth and the resulting modification of contact trajectory caused by the loss of material along the wheel tread. These results suggest a shift towards favouring load-based measurements over visual inspections.

Vehicle–track interaction involving unsupported sleepers has previously been analysed in [7] and [8], with particular focus on the effects of the number of voided sleepers, train speed and void depth. The results in [7] showed that the wheel–rail contact force increases with both the number of unsupported sleepers and the train speed, whereas no clear monotonic trend was observed for progressively increasing void depth. In [8], it was reported that, for a case involving three unsupported sleepers and train speed of 320 km/h, the maximum vertical wheel–rail contact force increases by 25%, while sleeper displacement and rail seat loads increase by a factor of four. However, the effect of impact loads generated by wheel defects was not studied.

The aim of this work is to analyse the effect of unsupported sleepers as an additional factor influencing the measured outputs of WILDs. The studied detector types, briefly described in Section 2, rely either on strain gauges, mounted on the side of the rail or through a device beneath it, or on fibre-optic sensors placed at the rail foot. Track dynamic signals representative of three commonly used WILDs are numerically simulated using the in-house software DIFF. The simulation model is described in Section 3. The methodology adopted in this study involves analysing how the original sensor signals are altered in the presence of void depths of up to 4 mm beneath two adjacent sleepers, before any post-processing used for deriving contact forces. This approach allows to systematically assess the sensitivity of the specific detector type to unsupported sleepers, as presented in Sections 4 and 5.

## 2 Wheel impact load detectors

The three detectors considered in this study are shown in Figure 1, and they are sorted in terms of chronological order of introduction on the Swedish railway network. The first one, (a), is a detector developed by Salient, now part of L.B. Foster [9], which relies on strain gauges placed on the rail web. The second detector, (b), is manufactured by Schenck [10] and is likewise based on strain measurements, although in this case the gauges are mounted through the use of specific weighing sleepers. The third system, (c), is produced by voestalpine Signaling [11] and uses fibre-optic sensors to measure the relative rotation between two fixed points on the foot of the same rail.

(a)

(b)

(c)

Figure 1: Wheel impact load detectors: (a) L.B. Foster (from [9]), (b) Schenck (photo by Matthias Asplund, Trafikverket), (c) voestalpine Signaling (from [11]).

In the first two cases, the measurement principle is based on converting strains into, respectively, vertical shear force and rail seat load. For the third detector type, the rail rotation is instead converted into bending moment from which the load is then derived. To accurately capture a complete wheel revolution and the dynamic effects induced by the passage of an entire train, multiple sensors must be installed and distributed within a certain length along the track (detector area). Moreover, calibration must be performed based on the known axle loads of the rolling stock operating on the line.

It is important to note that this study does not address the calibration procedures or post-processing routines implemented by the manufacturers, as this is proprietary information unknown to the authors. The primary aim is to assess the effect of unsupported sleepers within the detector area. To this end, simulations were performed to generate and analyse signals that mimic the behaviour of the various sensor types. The simulated outputs are the difference in shear force between two points within a sleeper bay, used to emulate the strain-based load measurement of the L.B. Foster detector, the rail seat load for the Schenck system, and the relative rail rotation in the case of the voestalpine Signaling device. The robustness of the detector outputs is investigated by comparing the variation in the simulated signals against a reference case, which consists of a wheel flat impact at the centre of a sleeper bay with no voided sleepers.

# 3 Model description

In this section, the numerical model used to simulate the vehicle–track interaction in the presence of a wheel flat and voided sleepers is presented. The model is structured into three components: the track, containing 60E1 rails discretely supported by sleepers on ballast; the vehicle, represented by four SJ57H freight wheels in two adjacent bogies from consecutive wagons, and the interaction between the two, as induced by a relative wheel–rail displacement. The dynamic interaction is solved using the in-house software DIFF by adopting an extended state-space vector approach with time-domain integration. This method allows to account for the non-linearities induced by the wheel flat irregularity and by the state-dependent track characteristics due to the presence of voided sleepers. More details of the model can be found in [12] and [13].

## 3.1 Track model

The track model is a finite element model representing one rail discretely supported by concrete sleepers on ballast with state-dependent properties, see Figure 2. To reduce computational time, geometric and loading symmetry about the track centreline is assumed, and consequently only half of the track is modelled. The model is considered to be periodic, except for the locations of the voided sleepers. It is composed of 80 sleeper bays with sleeper distance $L = 0.6$ m and eight rail beam elements per sleeper bay. The track length ensures that vibrational wave reflections induced by the clamped boundary conditions at the two rail ends are negligible in the central region.

The 60E1 rail is modelled by Rayleigh–Timoshenko beam finite elements with mass per unit length $m$ = 60 kg/m, bending stiffness $EI$ = 6.4 MN·m$^2$, shear stiffness $kGA$ = 250 MN and rotational inertia per unit length $mr^2$ = 0.24 kg·m. The half sleepers are represented by lumped masses with mass $M_{sl}$ = 150 kg connected to the rail via pads modelled with springs of stiffness $k_p$ = 120 MN/m and dashpots with viscous damping $c_p$ = 80 kN·s/m [14]. The ballast and subgrade are likewise modelled with lumped masses, springs, and dampers, under the assumption that the sleeper–ballast load transfer can be approximated by a conical distribution. The equations used to derive the input data are described in [15]. A lumped mass $M_b$ = 319 kg that models the ballast is connected to the half-sleeper mass $M_{sl}$ through a spring of stiffness $k_b$ = 239 MN/m and a dashpot of damping $c_b$ = 60 kN·s/m. The ballast mass is connected to rigid ground by a spring of stiffness $k_s$ = 75 MN/m and a dashpot of damping $c_s$ = 30 kN·s/m, representing the stiffness and damping of the soil. To model the interlocking of ballast particles, shear springs and dampers between ballast masses are introduced with stiffness $k_{ss}$ = 80 MN/m and damping $c_{ss}$ = 80 kN·s/m.

The equations of motion for the presented model are formulated in a state-space representation, with nodal displacements and velocities as state variables. The forces acting on the track are the wheel-rail contact forces, $F_{w/r}$, the gravitational load, $F_g$, and the state-dependent load associated with the voided sleepers, $F_{s/b}$. The latter is considered by applying equivalent external forces, represented through piecewise segmented characteristics of $F_{s/b}$, to the nodes of the unsupported sleepers and associated ballast masses [13], as described in Subsection 3.3.

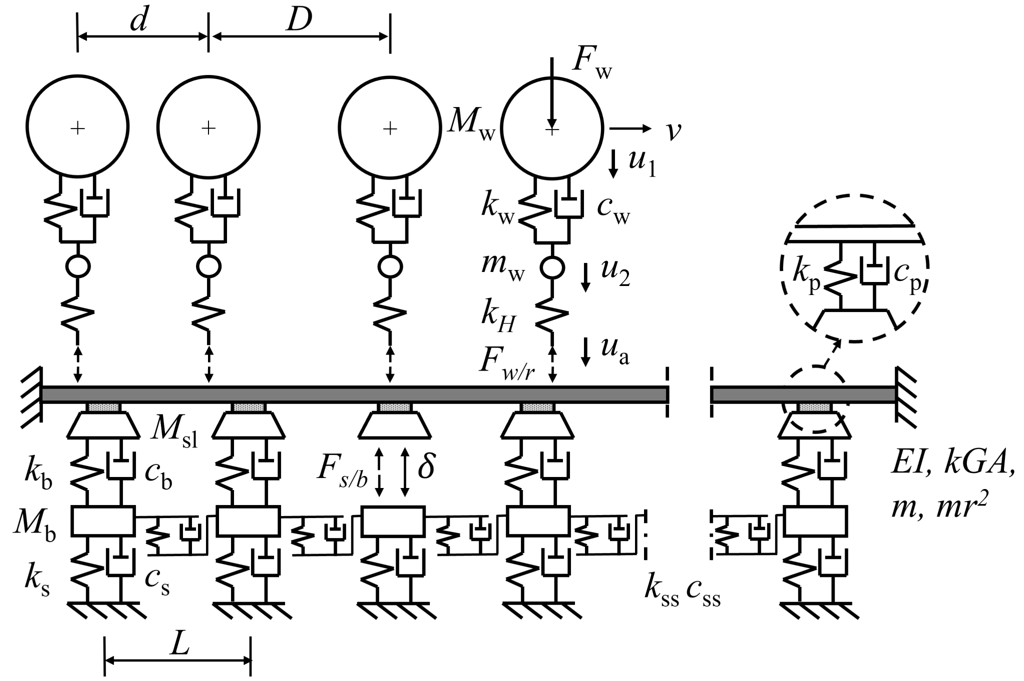


Figure 2: Vehicle–track interaction model with an unsupported sleeper.

## 3.2 Vehicle model

The vehicle is modelled as four lumped parameter units travelling at a constant speed $v$ from left to right along the track, as shown in Figure 2. These lumped parameters represent the four wheelsets mounted on two adjacent Y25 bogies belonging to consecutive wagons. This configuration is chosen to account for the increased loading on the track due to the close spacing of the wheelsets. A discretised vehicle model including only the wheelsets is deemed sufficient, because wheel flats excite frequencies that are significantly higher than the resonance frequencies associated with the lower vibration modes of the vehicle, owing to the filtering effect of the primary suspension.

The large mass $M_w$ = 712.5 kg corresponds to half of the mass of an SJ57H Swedish freight wheelset. The adopted parameters $m_w$ = 3 kg, $k_w$ = 1650 MN/m, and $c_w$ = 5.4 kN·s/m are non-physical values tuned to align the receptance of the model (i.e. the radial displacement of the wheel tread under a unitary load in the frequency domain) with that obtained from a detailed 3D finite element model of the wheelset [16]. The stiffness $k_H$ is a non-linear compression-only Hertzian stiffness of the wheel–rail contact. It is determined by assuming a wheel curvature of 1/0.45 m$^{-1}$, rail curvature = 0, transverse wheel curvature = 0, and a transverse rail curvature of 1/0.3 m$^{-1}$. The longitudinal distance between the two wheelsets on the same bogie is $d$ = 1.8 m, while the distance between wheelsets on consecutive wagons is $D$ = 3.5 m.

The resulting vehicle model is solved with respect to the three degrees of freedom associated with each wheelset: $u_1$ is the downward displacement of the mass $M_w$, $u_2$ is the downward displacement of the mass $m_w$, and $u_a$ is the downward displacement of a massless interfacial point representing the wheel–rail longitudinal contact position. The external forces acting on the wheelsets are the gravitational load $F_w$ (axle load 25 tonnes), and the wheel-rail contact forces, $F_{w/r}$, which are taken to be equal in magnitude and opposite in sign to those introduced in the track model.

## 3.3 Wheel–rail interaction

To implement the interaction between the track and vehicle models, constraint equations between each wheel and the rail must be formulated. As a consequence of the spatial discretisation of the rail, the moving wheel–rail contact forces, $F_{w/r}$, are transformed into stationary, time-variant forces. This is achieved at each time step by distributing their values to the two adjacent rail nodes using the shape functions adopted in the finite element formulation; full details are provided in [12].

The constraint equations can be formulated in a simplified expression as $u_a(x,t) = u_t(x,t) + u_{w/r}(x,t)$, where the displacement of the interfacial point $u_a(x,t)$ is set equal to the sum of the track displacement $u_t(x,t)$ and the prescribed relative wheel–rail displacement $u_{w/r}(x,t)$ at track coordinate $x$ and time $t$. An extended state-space equation for the train–track interaction system is obtained by assembling the equations of motion for the track and vehicle models plus the algebraic constraint equations, leading to the following first-order matrix formulation: $[A](z)\dot{z} + [B](z)z = F(z)$.

The state-space vector $z = [u_t^T, \dot{u}_t{}^T, u_a^T, u_b^T, \dot{u}_a{}^T, \dot{u}_b{}^T, \hat{F}_{w/r}]^T$ includes the displacements $u_t$ and velocities $\dot{u}_t$ of the track model, the displacements and velocities of the vehicle model (both the mass coordinates $u_b$ and the interfacial coordinates $u_a$), as well as the impulses of the wheel–rail contact forces $\hat{F}_{w/r}(t) = \int F_{w/r}(t)dt$.

The mixed force vector $F(z) = [F_{s/b}^T + F_g^T, 0^T, 0^T, F_w^T, 0^T, \dot{u}_{w/r}^T, \ddot{u}_{w/r}^T]^T$ contains the gravitational loads acting on the track, $F_g$, and on the vehicle, $F_w$, as well as the state-dependent sleeper–ballast contact force, $F_{s/b}$, through which the effect of unsupported sleepers is introduced. The term $u_{w/r}$ represents a prescribed irregularity function modelling the wheel trajectory due to a given wheel out-of-roundness profile.

The effect of the wheel flat is implemented by removing a section of the wheel's rolling circle profile, as shown in Figure 3(a). Instead of a perfect circular profile, a fresh wheel flat exhibits sharp edges and an initial length $L_o$, which can be related to the defect depth $d_f$ and the wheel radius $R$ through the chord theorem $L_o = \sqrt{8Rd_f - 4d_f^2}$. A fresh wheel flat rapidly evolves into a longer, rounded defect of the same depth but of length $L_f$. In this study, a rounded flat is implemented using an irregularity function $u_{w/r}$, which represents the wheel centre trajectory in the presence of the defect. As the wheel rolls along the longitudinal coordinate $\xi$, the wheel centre initially drops after the leading edge of the flat ($\xi = 0$) and subsequently rises again. This behaviour can be approximated using the following equations [17].

$$u_{w/r} = \begin{cases} 4d_f \left(\dfrac{\xi}{L_f}\right)^2, & 0 \leq \xi \leq \dfrac{L_f}{2} \\ 4d_f \left(\dfrac{L_f - \xi}{L_f}\right)^2, & \dfrac{L_f}{2} < \xi \leq L_f \end{cases} \tag{1}$$

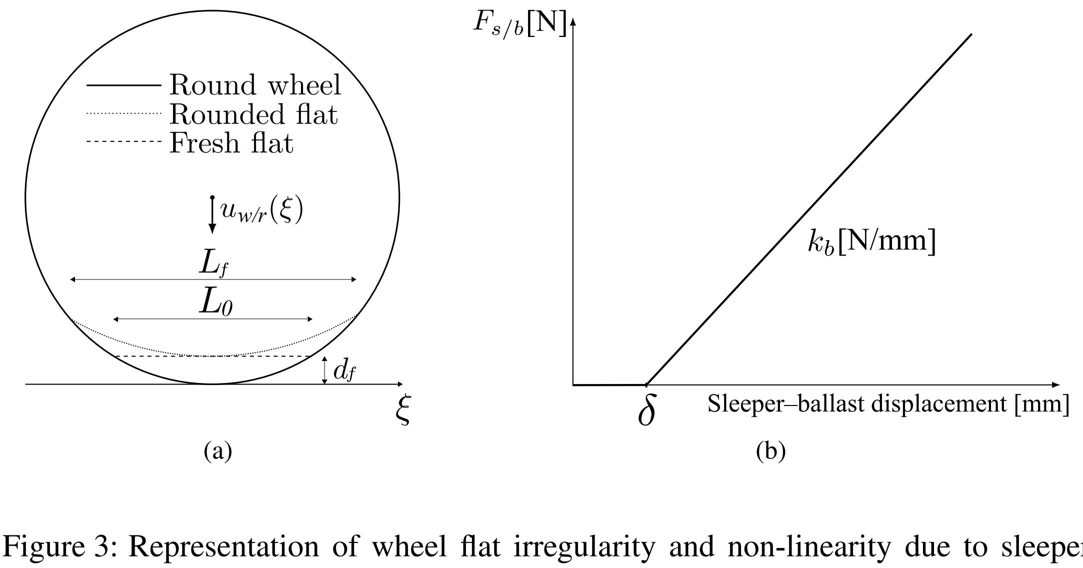


Figure 3: Representation of wheel flat irregularity and non-linearity due to sleeper void depth $\delta$: (a) wheel flat profile, (b) sleeper–ballast contact force.

The effect of unsupported sleepers is taken into account by introducing a piecewise segmented force characteristic, $F_{s/b}$, acting on the lumped masses representing the voided sleepers and corresponding ballast. This approach is commonly used in the literature, for example in [7]. No force is transmitted between the two components as long as the relative displacement of sleeper and ballast does not exceed a prescribed void depth $\delta$. Once this displacement threshold is reached, the force increases with the same ballast stiffness $k_b$ as in the case of fully supported sleepers. A schematic representation of the resulting force–displacement relationship is shown in Figure 3(b).

The initial displacement field of the track, resulting from the gravitational loads and the presence of unsupported sleepers, is obtained using the MATLAB® solver fsolve. Subsequently, the initial-value problem defined by the first-order state-space matrix formulation of the vehicle–track system is integrated using the moderately stiff differential equation solver ode23.

# 4 Results and discussion

The described model is used to simulate the signals associated with the working principles of the considered sensors. The reference case consists of a wheel flat located on the leading wheel, with length $L_f$ = 60 mm and depth $d_f$ = 1 mm, impacting at the midpoint of sleeper bay number 41, the centre of the track model, with no unsupported sleepers, at $v$ = 100 km/h. This combination of parameters is deliberately selected to induce a loss of wheel–rail contact. The reference is then compared with cases involving increasing void depths $\delta$ from 0 to 4 mm, at both ends of the considered sleeper bay: sleeper numbers 40 ($\delta_1$) and 41 ($\delta_2$). The sensitivity of the detectors to voided sleepers is assessed by evaluating the signal variations with respect to the reference.

## 4.1 Simulation results

To mimic the output from the sensors, before any post-processing (which is unknown to the authors), the signals shown in Figure 4 were simulated. Here, representative cases with zero, one, and two unsupported sleepers are illustrated. For the L.B. Foster detector, the shear forces were calculated at the nodes located at 1/8 and 7/8 of sleeper bay 41, approximating the positions of two strain gauge bridges. Their difference was used to estimate the wheel–rail contact force under static equilibrium assumptions (the effect of the rail inertia was neglected), as shown in Figure 4(a). For the Schenck detector, the rail seat load was evaluated at sleeper 40, as presented in Figure 4(b). For the voestalpine Signaling system, the relative rail rotation between the nodes at 6/8 and 7/8 of the sleeper bay was used to emulate the fibre-optic arrangement, as presented in Figure 4(c). The wheel–rail contact force of the first (damaged) wheel is plotted in Figure 4(d): only the impact within the analysed sleeper bay has been considered. The time-domain simulation provided outputs at a sampling frequency of 20 kHz, to ensure accurate resolution of the peaks induced by the wheel flat.

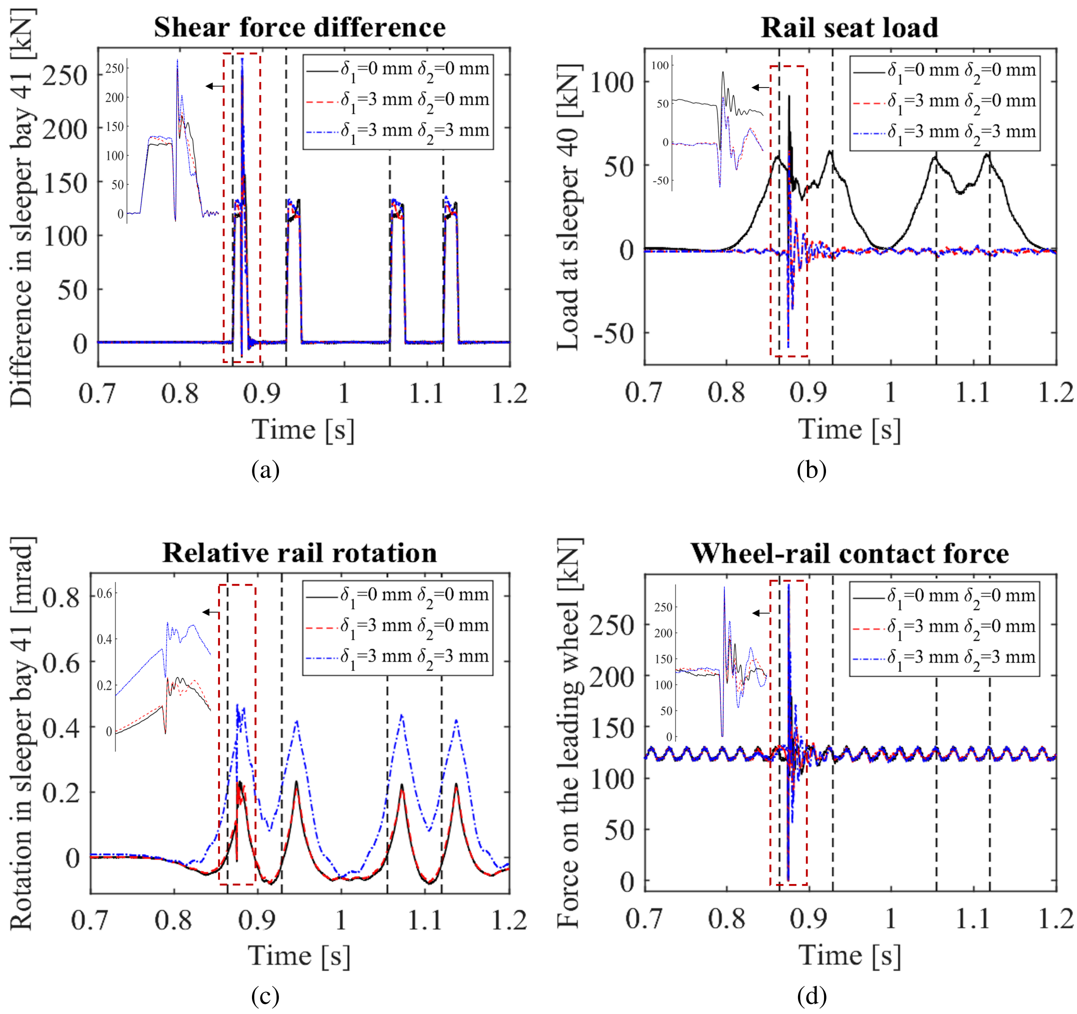


Figure 4: Simulation results: (a) shear force difference in sleeper bay 41, (b) rail seat load at sleeper 40, (c) relative rail rotation in sleeper bay 41, (d) wheel–rail contact force. Dashed vertical black lines indicate when each of the four wheels enters sleeper bay 41.

In Figure 4, the signals are presented for the fully supported reference track, a case where sleeper 40 is unsupported with a void depth of $\delta_1$ = 3 mm, and one case where both sleepers 40 and 41 are unsupported with $\delta_1 = \delta_2$ = 3 mm. These cases were selected to emphasise the noticed trends and signatures of the simulated signals. As a consequence of the working principle of each individual sensor, the characteristic signatures of wheel passages are clearly identifiable when a wheelset is travelling within a sleeper bay. The passage of each wheel is captured by an increase in the detector signals, and the wheel flat impact is detected as a distinct peak. The recorded signal decays to zero as the wheel moves away from the instrumented sleeper bay: the shear force difference rapidly drops to zero, while for the rail seat load and the relative rotation a longer transient is present. This is distinguishable in Figure 4 by observing the signal between the passages of two consecutive wheelsets. The described behaviour justifies the choice of simulating an impact in the middle of the bay, as well as the need to use multiple sensors in sequence to fully capture the wheel passages.

The peak values induced by the wheel flat do not exhibit a monotonic trend as the void depth increases. In the specific cases shown in Figure 4, when only $\delta_1$ is present, the peak values generated by the wheel defect for the contact force, relative rotation, and shear force difference, decrease compared with the reference case. In contrast, these magnitudes increase when both sleepers are voided. These results are valid with the exception of the rail seat load, for which the measured force decreases with the number of unsupported sleepers. In Figure 4(b), the passages of the second to fourth wheels are not detected in the presence of voided sleepers, because the vehicle-track interaction does not lead to a sleeper displacement sufficient to close the gap $\delta_1$.

The observed variations can be explained by the effects of the high-frequency excitation of the wheel flat impact and the low-frequency excitation induced by the unsupported sleepers. Together, these produce a wheel–rail interaction defined by a momentary loss of contact along with larger rail displacements due to the voided sleepers.

## 4.2 Influence of unsupported sleepers on detector signals

A comparison of the influence of unsupported sleepers on the sensitivity of the detected signals is carried out by calculating the relative percentage variation of the maximum values recorded within sleeper bay 41. This variation $\Delta_{i\%}$, relative to the case without unsupported sleepers, is computed as

$$\Delta_{i\%}(\delta_1, \delta_2) = \frac{\max(f_i(\delta_1, \delta_2, t)) - \max(f_i(\delta_1 = 0, \delta_2 = 0, t))}{\max(f_i(\delta_1 = 0, \delta_2 = 0, t))} * 100\% \tag{2}$$

where $f_i$ for $i$ = 1, 2, 3, 4 represents the shear force difference, the rail seat load, the relative rail rotation, and the wheel–rail contact force of the first wheel, respectively. The considered maximum value is always associated with the defect-induced peak.

Simulations were carried out for every combination of $\delta_1$ and $\delta_2$ within the range 0 - 4 mm with increments of 1 mm. The resulting values of percentage variation, $\Delta_{i\%}$, are presented in Figure 5. As a general trend, it is observed that progressively larger voids under sleepers 40 and 41 lead to increasing variations. However, it can be noted that beyond a certain void depth, the signals, and their corresponding maxima, converge to constant values, a result which was also observed in [18]. This plateau occurs between 2 and 3 mm when only one sleeper is unsupported, and shifts to between 3 and 4 mm when both sleepers are voided. With two unsupported sleepers, the track undergoes greater displacements, enabling it to bridge larger voids. The subsequent stabilisation arises because the vehicle–track interaction, at the considered speed, is no longer able to produce sufficient displacements to close the gaps beneath the sleepers. This results in no further change in the unsupported response.

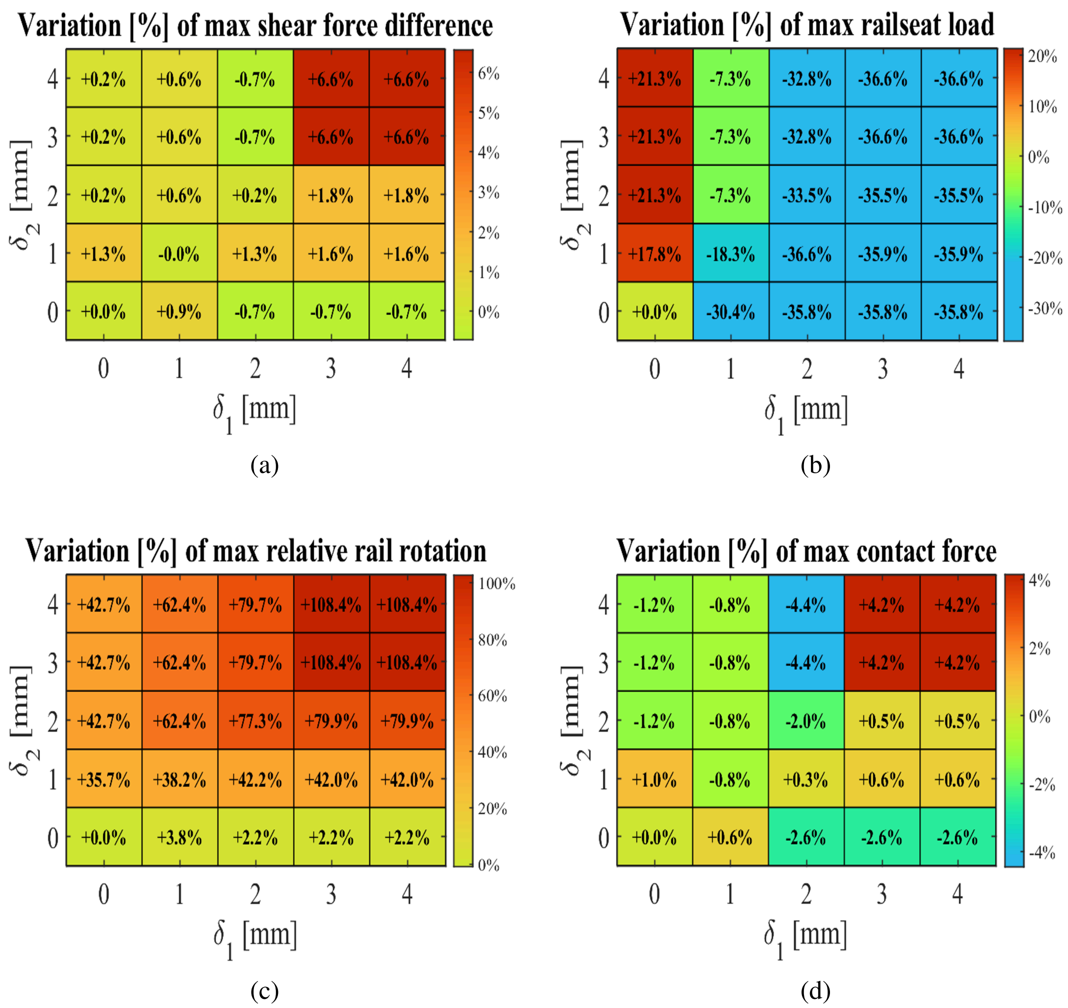


Figure 5: Variation [%] in maximum signal response relative to fully supported case: (a) shear force difference in sleeper bay 41, (b) rail seat load at sleeper 40, (c) relative rotation in sleeper bay 41, (d) wheel–rail contact force.

When comparing the detector signals, the maximum shear force difference, see Figure 5(a), most closely mirrors the variations observed for the contact force, see Figure 5(d). This similarity is expected, since the shear force signal is a quantity which, under equilibrium conditions, should reproduce the contact force reasonably well. Nevertheless, discrepancies arise both in the absolute peak values and in the trend behaviour. For example, with a gap of 4 mm applied to both $\delta_1$ and $\delta_2$, the shear force difference signal exhibits a +6.6% deviation from the reference case, compared with a +4.2% variation for the contact force. This discrepancy can be attributed to the omission of rail inertia in the processing of the shear force difference signal.

In Figure 5(b), when $\delta_1 = 0$ and $\delta_2 > 0$, an increase in the measured rail seat load is observed. This occurs because the applied vehicle load is redistributed to the sleepers adjacent to unsupported sleeper 41, a result also reported in [18]. In the remaining cases, where a gap beneath sleeper 40 is present, the simulated output is reduced, reflecting the diminished support and the altered load-transfer path. The rail seat load reaches values of up to +21.3% when $\delta_2$ is increased while no void is present beneath the instrumented sleeper, whereas it decreases to -36.6% when $\delta_1$ is also active.

The relative rotation signal, illustrated in Figure 5(c), shows only minor deviations from the reference case, when a void is present solely beneath the first sleeper ($\delta_1$). However, it is sensitive to changes in $\delta_2$, as the measurement location is closer to the second sleeper. Consequently, variations of up to +108.4% are observed. The increased rotation arises from the reduced vertical support provided by the sleepers, resulting in a longer effective span of unsupported rail.

In Figure 5(d), no monotonic trend in the maximum contact force can be observed. As discussed in Subsection 4.1, this behaviour occurs because of the combined effect of the wheel flat and the presence of voided sleepers. The largest identified increment, +4.2%, occurs when both sleepers in the sleeper bay are unsupported, as a consequence of a larger track deflection.

To summarise the comparisons of the unprocessed detector signals, the relative rail rotation generally increases when the track support is inadequate, whereas the rail seat load on an unsupported sleeper decreases. In contrast, the shear force difference more closely follows the contact force trend. However, it captures peak values only when the impact occurs within the sleeper bay, between the two mounted strain gauges.

# 5 Conclusions

A robust and reliable detection of wheel impact loads in the presence of damaged wheels is essential for ensuring the safety of both infrastructure and rolling stock. The sensors used for this purpose on the Swedish railway network are wayside detectors mounted either on the rail or on a sleeper, measuring strains or rail rotations that are subsequently processed into force estimates. Owing to their measurement principles, the unprocessed signals from such detectors are sensitive to the presence of unsupported sleepers. Numerical simulations have therefore been performed to replicate the raw detector signals of shear force difference, rail seat load, and relative rail rotation, considering a given wheel flat and train speed, while progressively increasing the voids beneath the two sleepers within a sleeper bay.

A comparison with a reference case featuring fully supported sleepers resulted in the following observations. For the maximum wheel–rail contact force, the resulting trend is influenced by the combined effect of the high-frequency excitation generated by the wheel flat impact and the low-frequency response associated with unsupported sleepers. No monotonic trend was observed with increasing void depths, and a stabilisation of values occurs once the sleeper displacement becomes insufficient to close the full gap. The greatest increase, +4.2%, occurs when both sleepers are unsupported with large voids. The shear force difference signal is capable of capturing and mirroring the trend of the contact force when the impact occurs within the sleeper bay. The maximum variation from the reference case is +6.6%. However, when an impact occurs outside of a pair of strain gauges within a given sleeper bay, the associated effects are not captured. Voids beneath both sleepers within a sleeper bay lead to a reduction of rail seat load signal for the instrumented sleeper down to -36.6%, whereas a gap beneath only the adjacent sleeper results in a redistribution of load to the instrumented sleeper and an increase of the signal of up to +21.3%. Due to the increased track flexibility in the presence of unsupported sleepers, the simulated rail rotation signals tend to increase, reaching deviations of up to +108.4%.

In general, all three detector types are able to detect wheel passages and peak loads when the impact occurs within the active detector region. Due to their measurement principles, the voestalpine Signaling detector, relying on relative rail rotation, and the Schenck detector, based on rail seat load, are the most affected by unsupported sleepers: reduced track stiffness leads to larger rail rotations, while changes in the sleeper–ballast interaction influence the recorded rail seat load. The L.B. Foster detector, which relies on shear force difference, follows the contact force trend more accurately, but its performance is strongly dependent on the location of the impact as it can capture forces only within the region bounded by the two strain gauge positions. These findings highlight the importance of proactive maintenance planning for WILDs, particularly with regard to the rectification of track geometry irregularities and unsupported sleepers through tamping and track stabilisation. Unless the influence of voided sleepers is explicitly accounted for by appropriate post-processing of the measured signals, such defects can significantly affect detector performance and undermine the reliability of impact load assessment.

## Acknowledgements

The current study is part of the activities within CHARMEC Chalmers Railway Mechanics. Funded by the European Union. Views and opinions expressed are however those of the authors only and do not necessarily reflect those of the European Union or the Europe's Rail Joint Undertaking. Neither the European Union nor the granting authority can be held responsible for them. The project FP5-TRANS4M-R is supported by the Europe's Rail Joint Undertaking and its members. Additional funding has been provided by the Swedish innovation agency VINNOVA, contract no. 2023-01218.

# References

[1] S. Iwnicki, J.C.O. Nielsen, G. Tao, ”Out-of-round railway wheels and polygonisation”, Vehicle System Dynamics, 61(7), 1787–1830, 2023.

[2] M. Maglio, T. Vernersson, J.C.O. Nielsen, A. Ekberg, E. Kabo, ”Influence of railway wheel tread damage on wheel–rail impact loads and the durability of wheelsets”, Railway Engineering Science 32, 20–35, 2024.

[3] Trafikverket, “Detektorer. Hantering av larm samt åtgärder efter konstaterade skador”, (“Detectors. Handling of alarms and measures following ascertained damages”, in Swedish), TDOK 2020:0074 v2.0, 2021.

[4] K. Mattsson, J.C.O. Nielsen, L. Fehrlund, M. Maglio, T. Vernersson, ”On way-side detector measurement of wheel–rail impact loads induced by wheel flats – Data analysis, alarm levels and regulations”, in J. Pombo, (Editor), Proceedings of the Sixth International Conference on Railway Technology: Research, Development and Maintenance, Civil-Comp Press, Edinburgh, UK, Online volume: CCC 7, Paper 7.10, 2024.

[5] M. Maglio, N. Lagata, K. Mattsson, J.C.O. Nielsen, T. Vernersson, ”Wheel-rail impact loads induced by wheel flats – Simulation model using data from 3D laser-scanned wheel tread defects”, Proceedings of the 29th Symposium of the International Association of Vehicle System Dynamics, IAVSD, Shanghai, China, August 2025.

[6] M. Asplund, P. Söderström, “Detector response from a defective wheel”, Wear, 542–543, 205282, 2024.

[7] S. Zhang, X. Xiao, Z. Wen, X. Jin, ”Effect of unsupported sleepers on wheel/rail normal load”, Soil Dynamics and Earthquake Engineering, 28, 662-673, 2008.

[8] J.Y. Zhu, D.J. Thompson, C.J.C. Jones, ”On the effect of unsupported sleepers on the dynamic behaviour of a railway track”, Vehicle System Dynamics, 49(9), 1389-1408, 2011.

[9] https://lbfoster.com/assets/lbfoster-brochure-wildiv-1-22-26_mbf.pdf.

[10] R. Müller, M. Speyerer, Multirail® Wheelscan Banverket, Schweden Version 1.1, Schenck Process GmbH, Darmstadt, 70 pp, 2006.

[11] D. Venekamp, PHOENIX$^{MDS}$ WIM/WDD Function Description Revision 03.1, voestalpine SIGNALING Siershahn GmbH, Siershahn, 37 pp, 2019.

[12] J.C.O. Nielsen, A. Igeland, ”Vertical dynamic interaction between train and track - Influence of wheel and track imperfections”, Journal of Sound and Vibration, 187(5), 825-839, 1995.

[13] J.C.O. Nielsen, J. Oscarsson, ”Simulation of dynamic train–track interaction with state-dependent track properties”, Journal of Sound and Vibration, 275, 512-532, 2004.

[14] D.J. Thompson, W.J. van Vliet, ”Measurements of the high frequency dynamic properties of Swedish rail pads”, Technical Report, TPD-HAG-RPT-960066, TNO Institute of Applied Physics, Delft, The Netherlands, 1996.

[15] W.M. Zhai, K.Y. Wang, J.H. Lin, ”Modelling and experiment of railway ballast vibrations”, Journal of Sound and Vibration, 270, 673-683, 2004.

[16] J.C.O. Nielsen, G. Lombaert, S. François, ”A hybrid model for prediction of ground-borne vibration due to discrete wheel/rail irregularities”, Journal of Sound and Vibration, 345, 103-120, 2015.

[17] T.X. Wu, D.J. Thompson, ”A hybrid model for the noise generation due to railway wheel flats”, Journal of Sound and Vibration, 251(1), 115-139, 2002.

[18] J.J. Zhu, A.K.W Ahmed, S. Rakheja, A. Khajepour, ”Development of a vehicle–track model assembly and numerical method for simulation of wheel–rail dynamic interaction due to unsupported sleepers”, Vehicle System Dynamics, 48(12), 1535–1552, 2010.